Journal of Luminescence 175 (2016) 260–266

Contents lists available at ScienceDirect

Journal of Luminescence

journal homepage: www.elsevier.com/locate/jlumin

Full Length Article

Stokes and anti-Stokes luminescence from cubic elpasolite Cs_2NaYF_6 crystals doped with Er^{3+} and Yb^{3+} ions

P.A. Loiko [a,*], N.M. Khaidukov [b], J. Méndez-Ramos [c], E.V. Vilejshikova [a], N.A. Skoptsov [a], K.V. Yumashev [a]

[a] Center for Optical Materials and Technologies (COMT), Belarusian National Technical University, 65/17 Nezavisimosti Ave., Minsk 220013, Belarus
[b] N.S. Kurnakov Institute of General and Inorganic Chemistry, 31 Leninskii Prospekt, Moscow 119991, Russia
[c] Departamento de Física, Universidad de La Laguna, Tenerife, 38206 La Laguna, Spain

ARTICLE INFO

Article history:
Received 29 October 2015
Received in revised form
31 January 2016
Accepted 22 February 2016
Available online 15 March 2016

Keywords:
Elpasolite crystals
Erbium
Ytterbium
Luminescence
Up-conversion

ABSTRACT

Er^{3+} and Yb^{3+} doped cubic elpasolite Cs_2NaYF_6 crystals including stoichiometric compositions Cs_2NaErF_6 and Cs_2NaYbF_6 have been synthesized under hydrothermal conditions. Absorption, stimulated-emission and gain cross-sections spectra have been determined for the $^2F_{5/2}\rightarrow{}^2F_{7/2}$ (Yb^{3+}) and $^4I_{13/2}\rightarrow{}^4I_{15/2}$ (Er^{3+}) transitions at room-temperature. The maximum σ_{SE} values are 1.8×10^{-21} cm^2 at 993 nm (Yb^{3+}) and 3.8×10^{-21} cm^2 at 1535 nm (Er^{3+}). Elpasolite crystals provide exceptionally long radiative lifetimes of the excited-states for both ions, namely $\tau(^2F_{5/2})$=6.3 ms and $\tau(^4I_{13/2})\sim$32 ms for 10 at% Yb^{3+}:Cs_2NaYF_6 and 10 at% Er^{3+}:Cs_2NaYF_6 which can be used in high pulse energy Q-switched lasers. Up-conversion luminescence has been studied for Er^{3+} doped and Er^{3+}, Yb^{3+} codoped Cs_2NaYF_6 crystals.

1. Introduction

Halide compounds having the elpasolite structure can be described by a general formula A_2BMX_6 where A and B are monovalent alkali ions provided that the ionic radius of A is greater than that of B, M stands for trivalent metal ions, which can be Al, Sc, transition elements and rare earth elements, and X is a halogen [1]. The elpasolite compounds crystallize in the face-centered cubic space group Fm3m [2] and can be described as double perovskites. In the structure the A alkali cations are located in the cuboctahedral sites whereas the B alkali cations and the M trivalent metal ions regularly alternate along the unit cell axes in octahedral sites. Accordingly, the MX_6 octahedra are perfectly cubic with O_h site symmetry for trivalent metal ions, while the MX_6 octahedra do not share halide ions with each other, i.e. the elpasolite structure is characterized by the isolated MX_6 octahedra. In addition, as all the halide compounds, elpasolites are materials with low-phonon energy.

The above mentioned peculiarities of elpasolite hosts lead to a significant reduction of the multiphonon relaxation rates for optically active rare earth (RE) ion dopants, which allows for an increased lifetime of some excited levels that can relax radiatively or can store energy for further up-conversion and cross-relaxation as well as provide relatively low concentration quenching of luminescence, which allows obtaining efficient luminescence in A_2BMX_6 containing high trivalent RE ion concentrations up to 100 at%.

To date, some spectroscopy data for several RE ions (Er^{3+}, Yb^{3+}, Tm^{3+}, Eu^{3+}) doped into the Cs_2NaYF_6 compound have been published; however, characterization of these materials is far from completeness mainly due to the difficulty of synthesizing optical quality crystals of elpasolites in general and Cs_2NaYF_6 in particular. For example, VUV 5d–4f luminescence of Er^{3+} ions, including a stoichiometric Cs_2NaErF_6 compound, has been studied followed by crystal field calculations for Er^{3+} ions [3,4]. Near-IR ($\sim$2.7 μm) emission of Er^{3+} ions in Cs_2NaYF_6 has been also investigated and the lifetime of the $^4I_{11/2}$ excited-state has been detected to be as long as $\sim$1 ms at room-temperature for highly-doped ($>$10 at%) samples [5]. Absorption and emission as well as crystal field analysis for Yb^{3+} ions in Cs_2NaYbF_6 has been reported [6–8]. In particular, very long lifetime of the Yb^{3+} excited-state, $\tau(^2F_{5/2})$= 5.63 ms, at room-temperature is observed for Cs_2NaYbF_6. Some spectroscopic peculiarities of Tm^{3+} ions in Cs_2NaYF_6 have been also studied [3,6,9] and crystal field calculations for a Tm:Cs_2NaYF_6 crystal have been performed [10]. The spectroscopic properties of Eu^{3+} and Tb^{3+} ions doped into Cs_2NaYF_6 have been investigated as well [11–13].

* Corresponding author.
E-mail address: kinetic@tut.by (P.A. Loiko).

http://dx.doi.org/10.1016/j.jlumin.2016.02.025
0022-2313/

The fluoride cubic elpasolite Cs_2NaYF_6 is isostructural with the chloride elpasolite Cs_2NaYCl_6, that has been extensively studied as an low phonon energy host for optically active ions of 3d, 4f and 5f elements, for example Er^{3+} [14,15]. In particular, Cs_2NaYCl_6 crystals doubly doped with Er^{3+} and Yb^{3+} have been studied as the near-IR-to-visible frequency converters [16,17] based on photon upconversion processes [18]. As a result of upconversion mechanisms, Er^{3+}–Yb^{3+} ion pairs can convert near-IR (~1 μm) emission of InGaAs laser diodes to green and red light. On the other hand, Cs_2NaYF_6 is harder and less moisture-sensitive than Cs_2NaYCl_6. Thus, the study of visible emissions in Er^{3+} and Yb^{3+} ions doped Cs_2NaYF_6 crystals is of practical interest for developing photon upconverters. High efficiency of up-conversion in the cubic elpasolite Cs_2NaYF_6 can be achieved due to the low value of the maximum phonon frequency which is 468 cm^{-1} [11]. This value is higher than that for Cs_2NaYCl_6 (285 cm^{-1}) [19] but it is acceptable for energy storage on excited levels. In addition, long lifetimes of the first excited-states of Er^{3+} and Yb^{3+} ions observed for highly-doped Cs_2NaYF_6 crystals indicate their potential for generation of high pulse energies in passively Q-switched near-IR lasers.

In the present paper, the data on optical absorption, near-IR and visible f–f emissions of Cs_2NaYF_6 crystals doped with Er^{3+} and Yb^{3+} ions as well as Cs_2NaErF_6 and Cs_2NaYbF_6 are reported.

2. Experimental

Crystals of cubic elpasolite Cs_2NaYF_6 doped with Er^{3+} and Yb^{3+} ions as well as Cs_2NaErF_6 and Cs_2NaYbF_6 were grown under hydrothermal conditions. For hydrothermal experiments, copper-insert lined autoclaves with a volume of ~40 cm^3 were utilized, and the inserts were separated by perforated diaphragms into synthesis and crystallization zones. The fluoride crystals were synthesized by a direct temperature-gradient method as a result of the reaction of the aqueous solutions containing 35–40 mol% CsF and 8–10 mol% NaF with oxide mixtures $(1-x)Y_2O_3-xLn_2O_3$ (Ln=Er and Yb) at a temperature of ~750 K in the synthesis zone, a temperature gradient along the reactor body of up to 3 K/cm, and a pressure of ~100 MPa. Under these conditions, spontaneously nucleated crystals of up to 0.5 cm^3 were grown in the upper crystallization zone of the autoclave for 200 h. The purities of the utilized rare earth oxides were 99.99%.

The structure type and phase purity of synthesized samples were characterized with conventional powder X-ray diffraction (XRD) technique and powder XRD patterns were obtained by using a Bruker D8 Advance X-Ray powder diffractometer with Cu Kα radiation.

Absorption spectrum was measured for 10 at% Er^{3+} and 10 at% Yb^{3+} doped Cs_2NaYF_6 crystals with a Varian CARY 5000 spectrophotometer (the spectral bandwidth, SBW, was 0.1 nm). Thin polished platelets (~1 mm) of crystals were used.

Luminescence spectra were measured with a lock-in amplifier, a monochromator MDR-23 (SBW ~0.1 nm) and Hamamatsu G5851 and C5460-01 photodetectors. The spectral sensitivity of the set-up was accurately determined with a halogen lamp with calibrated spectral power density. Near-IR luminescence and up-conversion luminescence (UCL) of Er^{3+} and Yb^{3+} ions was excited by InGaAs laser diode emitting at ~960 nm (excitation to the Er^{3+} $^4I_{11/2}$ state or Yb^{3+} $^2F_{5/2}$ state). Excitation light was focused on a sample in a ~100 μm spot; the maximum power density was ~40 kW/cm^2. Luminescence was also excited at ~355 and ~520 nm (excitation to the $^2G_{9/2}$ and $^2H_{11/2}$ states of Er^{3+}, respectively) and a ns optical parametric oscillator (OPO) Lotis TII LT-2214 was used. CIE chromaticity coordinates of phosphors were calculated by using the photoluminescence data.

For the studies of luminescence decay of Yb^{3+} ions, OPO with the pulse duration of ~20 ns was tuned to 960 nm. Luminescence was collected by a wide-aperture lens and re-imaged to the input slit of a monochromator MDR-12 (tuned to 1020 nm, SBW ~1 nm); then it was detected with a fast Hamamatsu G5851 photodetector (response time, < 100 ns) and a 500 MHz Textronix TDS-3052B digital oscilloscope. To avoid the reabsorption loss, studied crystals were finely powdered and immersed in glycerin (~5 wt% powder content).

All spectroscopic studies were performed at room temperature.

3. Results and discussion

The X-ray phase analysis has confirmed that all the synthesized compounds are single-phase samples containing only the cubic elpasolite phases, space group Fm3m, $Z=4$ (ICDD PDF Cards: 00-020-1214; 00-021-0221; 00-021-0224) [1]. X-ray diffraction patterns of Cs_2NaYF_6, Cs_2NaErF_6 and Cs_2NaYbF_6 are showed in Fig. 1 and they can be indexed with a cubic cell with the lattice parameter, $a=9.057$ Å, 9.045 Å and 9.016 Å, respectively. Lattice parameter (a), volume of the unit cell (V), density (ρ) and concentration (N) of the Y^{3+}, Er^{3+} and Yb^{3+} ions which have been obtained from the X-ray diffraction studies for these compounds are summarized in Table 1. One can see that there is a marginal change in cell parameters due to differences in rare earth ionic radii and it should be also noted that the unite cell parameters determined in this study are notably less than those tabulated in [1].

An absorption spectrum measured for a 10 at% Er^{3+}:Cs_2NaYF_6 crystal is shown in Fig. 2. For the $^4I_{15/2}\rightarrow{}^4I_{11/2}$ transition, the peak absorption cross-section is $\sigma_{abs}=0.07\times10^{-21}$ cm^2 at 963 nm. The full width at half maximum (FWHM) for this band is ~24 nm. Such low absorption determines low efficiency for the excitation of Er^{3+} ions by using InGaAs diodes. Indeed, for the stoichiometric Cs_2NaErF_6 crystal, the corresponding peak absorption coefficient is α ~0.37 cm^{-1}, which means that the absorption of diode emission is not complete even for a few mm-thick crystal. For the $^4I_{15/2}\rightarrow{}^4I_{13/2}$ transition that is typically used for the in-band excitation of

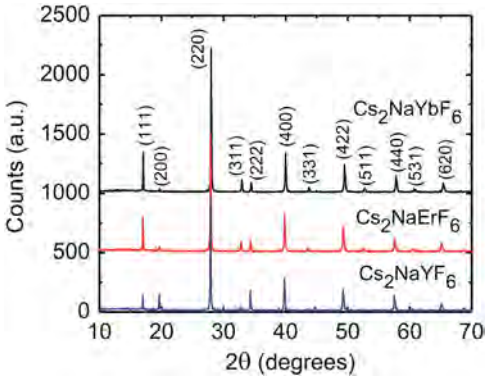

Fig. 1. X-ray diffraction patterns for Cs_2NaYF_6, Cs_2NaErF_6 and Cs_2NaYbF_6 crystals; numbers on the graph represent the Miller indices, (hkl).

Table 1
Lattice parameter (a), unit cell volume (V), calculated density (ρ) and absolute concentration of rare earth ions (N) for cubic elpasolites (space group: Fm3m, $Z=4$).

Composition	a, Å	V, Å^3	ρ, g/cm^3	N, at/cm^3
Cs_2NaYF_6	9.057	742.9	4.42	5.38×10^{21}
Cs_2NaErF_6	9.045	740.0	5.15	5.41×10^{21}
Cs_2NaYbF_6	9.016	732.9	5.24	5.46×10^{21}

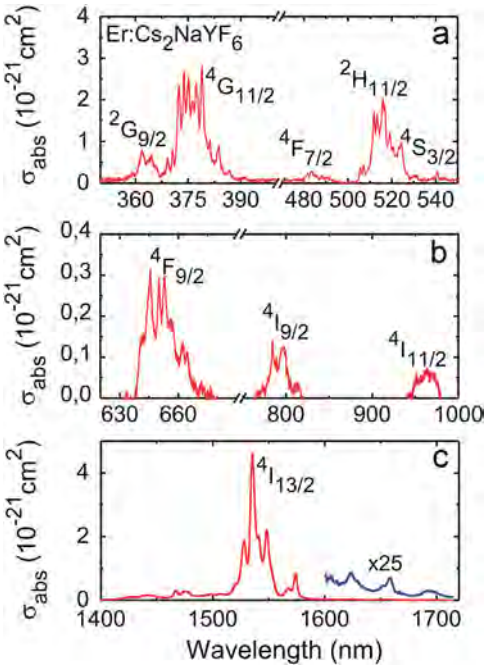

Fig. 2. Absorption cross-section spectra for a 10 at% Er^{3+}:Cs_2NaYF_6 crystal.

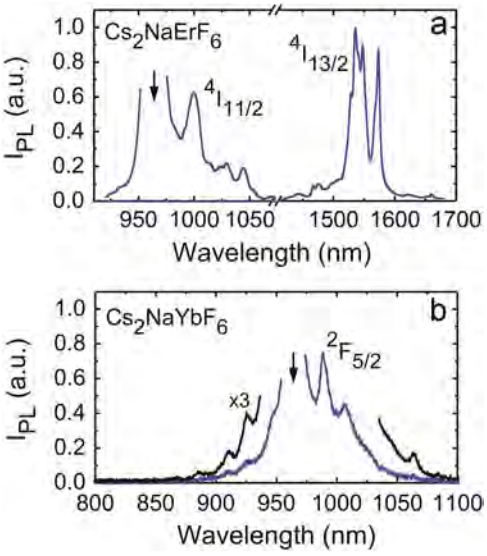

Fig. 3. Near-IR emission spectra of Cs_2NaErF_6 (a) and Cs_2NaYbF_6 (b) crystals; excitation wavelength is denoted by *arrow* (960 nm).

Er^{3+} ions, the absorption is much stronger, $\sigma_{abs}=4.6\times10^{-21}$ cm^2 at 1532.2 nm. The FWHM of this band is 5.4 nm.

Near-IR emissions of Er^{3+} ions have been studied under 960 nm excitation by using a stoichiometric Cs_2NaErF_6 crystal. The luminescence band related to the Er^{3+} $^4I_{13/2}\rightarrow{}^4I_{15/2}$ transition spans from ~1.4 to 1.68 μm, see Fig. 3(a). The band in the 920–1060 nm spectral range is attributed to the $^4I_{11/2}\rightarrow{}^4I_{15/2}$ transition of Er^{3+} ions.

Emission of Er^{3+} ions at ~1.5 μm is eye-safe and interesting for laser operation. To calculate the corresponding stimulated-emission cross-sections σ_{SE} spectra, two methods can be used. The first one is the reciprocity method [20]:

$$\sigma_{SE}(\lambda)=\sigma_{abs}(\lambda)\frac{Z_1}{Z_2}\exp\left(-\frac{hc/\lambda-E_{ZL}}{kT}\right), \quad (1)$$

where Z_1 and Z_2 are the lower and upper manifold partition functions, respectively, E_{ZL} is the energy corresponding to the zero phonon line, h is the Planck constant, c is the speed of light, λ is the light wavelength, k is the Boltzmann constant and T is the crystal temperature (room-temperature). Partition functions are determined as:

$$Z_m=\sum_k g_k^m\exp(-E_k^m/kT), \quad (2)$$

where $m=1, 2$; g_k^m is the degeneration of the sublevel having the number k and the energy E_k^m measured from the lower sublevel of the corresponding multiplet. The set of E_k^m values for the $^4I_{15/2}$ and $^4I_{13/2}$ states of Er^{3+} ions in the Cs_2NaYF_6 crystal [4] is listed in Table 2.

Calculation of σ_{SE} with the reciprocity method is beneficial as it does not require the information about the radiative lifetime τ_{rad} of the emitting state as well as direct measurement of the emission spectrum which can be changed as a result of the reabsorption loss. The obtained results are shown in Fig. 4(a). The maximum σ_{SE} value is 3.8×10^{-21} cm^2 at 1532.2 nm. This value is lower than the typical peak σ_{SE} values for the Er^{3+} $^4I_{13/2}\rightarrow{}^4I_{15/2}$ transition in widespread oxide and fluoride laser hosts, $0.5–1\times10^{-20}$ cm^2 [21]. In the spectral range where laser operation is expected, the maximum σ_{SE} value is 1.5×10^{-21} cm^2 at 1574.1 nm. Radiative lifetime of the Er^{3+} emitting state ($^4I_{13/2}$) can be

Table 2
Energies of Stark sub-levels for the ground-states and the first excited-states of Er^{3+} and Yb^{3+} in Cs_2NaYF_6 crystals [4,8].

Multiplet (Yb^{3+})	Sub-levels, cm^{-1}	Multiplet (Er^{3+})	Sub-levels, cm^{-1}
$^2F_{7/2}$	3	$^4I_{15/2}$	0
	324		25
	656		57
			259
			287
$^2F_{5/2}$	10,389	$^4I_{13/2}$	6492
	11,109		6517
			6532
			6682
			6686

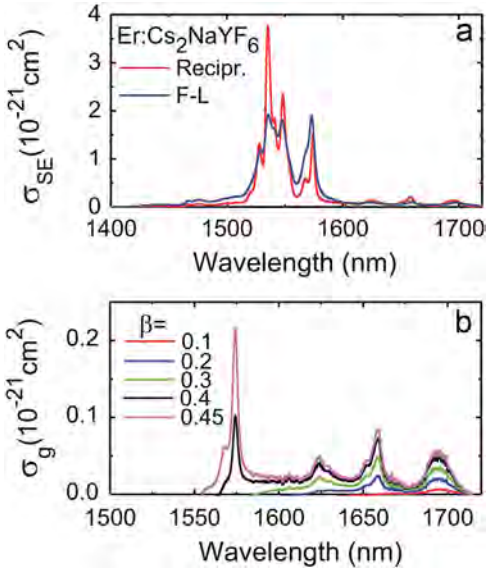

Fig. 4. (a) Stimulated-emission cross-sections spectra calculated with the reciprocity and F-L methods for a 10 at% Er^{3+}:Cs_2NaYF_6 crystal, (b) gain cross-sections [$\sigma_g=\beta\sigma_{SE}-(1-\beta)\sigma_{abs}$] spectra, $\beta=N_2/N$ is the inversion ratio.

estimated from the so-called modified reciprocity method (n is the crystal refractive index) [22]:

$$\tau_{rad} = \frac{1}{8\pi n^2 c}\frac{Z_2}{Z_1}\frac{\exp(-E_{ZL}/kT)}{\int \lambda^{-4}\sigma_{abs}(\lambda)\exp(-hc/(kT\lambda))d\lambda}. \quad (3)$$

For Er^{3+}:Cs_2NaYF_6 crystal, $\tau_{rad}(^4I_{13/2})$ has been determined to be $\sim 32 \pm 2$ ms. Previously, lifetime of this state was measured for 1 at% Er^{3+}:Cs_2NaYF_6 crystal only at cryogenic temperature (4 K), $\tau(^4I_{13/2}) \sim 100$ ms [5] and this value can be considered as a radiative one at low temperatures, as the reabsorption for such crystal doping is nearly vanishing. Such long values are inherent for all the elpasolite crystals [14]. In particular, $\tau(^4I_{13/2}) = 22$ ms for a cubic $Cs_2NaErCl_6$ crystal [23]. Independent estimation of the τ_{rad} for Er^{3+}:Cs_2NaYF_6 crystal can be done with the Judd–Ofelt modeling that will be performed in a separate study.

Using the measured emission spectrum $W(\lambda)$, Fig. 3(a), and the determined radiative lifetime $\tau_{rad}(^4I_{13/2})$, it is possible to calculate a stimulated-emission cross-sections spectrum for the $^4I_{11/2} \rightarrow {}^4I_{15/2}$ transition with the Füchtbauer–Ladenburg (F–L) equation [24]:

$$\sigma_{SE}(\lambda) = \frac{\lambda^5}{8\pi n^2 \tau_{rad} c}\frac{W(\lambda)}{\int \lambda W(\lambda) d\lambda}. \quad (4)$$

The obtained results are shown in Fig. 4(a) and they are in good agreement with the ones from the reciprocity method, considering strong reabsorption at short wavelengths.

For assessing the prospects of elpasolite crystals to lasers, a useful parameter is the gain cross-section, σ_g:

$$\sigma_g(\lambda) = \beta\sigma_{SE}(\lambda) - (1-\beta)\sigma_{abs}(\lambda), \quad (5)$$

where β is the inversion ratio, $\beta = N_2/N_0$ where N_2 and N_0 are the numbers of ions in the upper laser level and the overall number of ions, respectively. Gain spectra for a 10 at% Er^{3+}:Cs_2NaYF_6 crystal are shown in Fig. 4(b). For these calculations, we used stimulated-emission cross-sections spectra obtained with the reciprocity method. For low inversion ratios ($\beta < 0.4$), laser operation is expected at several wavelength, $\sim$1624, 1658 or 1694 nm. For high inversion ratios, the peak centered at 1574 nm dominates in the spectrum.

An absorption spectrum measured for a 10 at% Yb^{3+}:Cs_2NaYF_6 crystal is shown in Fig. 5(a) representing the $^2F_{5/2} \rightarrow {}^2F_{7/2}$ transition of Yb^{3+} ions. The peak absorption cross-section is $\sigma_{abs} = 1.3 \times 10^{-21}$ cm^2 at 962.0 nm. Thus, Cs_2NaYF_6 crystals containing both Er^{3+} and Yb^{3+} ions provide significant improvement of the excitation efficiency under using InGaAs laser diodes. In particular, the peak absorption coefficient for the stoichiometric Cs_2NaYbF_6 crystal, $\alpha = 6.9$ cm^{-1} and FWHM for this band is 5.2 nm.

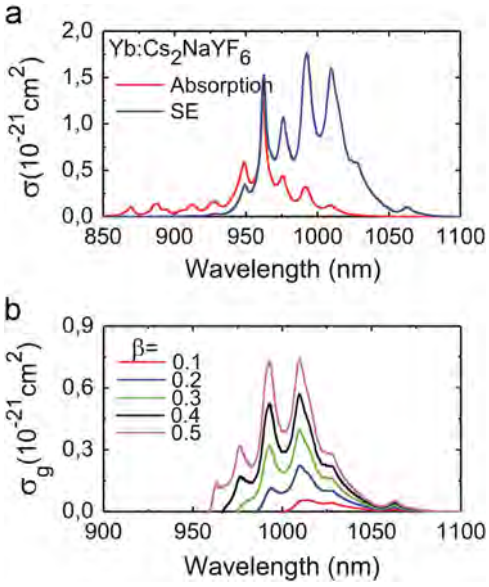

Fig. 5. (a) Absorption and stimulated-emission cross-sections spectra for a 10 at% Yb^{3+}:Cs_2NaYF_6 crystal, (b) gain cross-sections [$\sigma_g = \beta\sigma_{SE} - (1-\beta)\sigma_{abs}$] spectra, $\beta = N_2/N$ is the inversion ratio.

The stimulated-emission cross-sections spectrum for a 10 at% Yb^{3+}: Cs_2NaYF_6 crystal has been calculated with the reciprocity method, Eq. (1). The spectrum is shown in Fig. 5(a) and the energies of Stark sub-levels for the $^2F_{5/2}$ and $^2F_{7/2}$ states of Yb^{3+} ions used for calculations are listed in Table 2 [8]. The maximum σ_{SE} value is $\sim 1.8 \times 10^{-21}$ cm^2 at 992.4 nm. Emission of Yb^{3+} ions spans from $\sim$920 to 1080 nm. Thus, the tuning range wider than 100 nm is expected under using this crystal as a laser gain medium. This is in agreement with the near-IR emission spectrum of the Cs_2NaYbF_6 crystal measured directly under 960 nm excitation and shown in Fig. 3(b).

The radiative lifetime of the $^2F_{5/2}$ state of Yb^{3+} ions in the Cs_2NaYF_6 crystal determined from the modified reciprocity method, Eq. (3), is $\tau_{rad}(^4I_{13/2}) = 6.4$ ms. This value is in close agreement with the decay time of Yb^{3+} emission measured directly for a powdered 10 at% Yb^{3+}:Cs_2NaYF_6 composition, $\tau = 6.3$ ms. The corresponding decay curve is shown in Fig. 6 and it is clearly single-exponential. For a stoichiometric Cs_2NaYbF_6 crystal, similar measurement yields $\tau = 5.7$ ms, which is close to the previously reported value [6], $\tau = 5.63$ ms. Thus, the anomalously weak concentration quenching is observed for Yb^{3+}: Cs_2NaYF_6 crystals. Determined lifetimes are at least two times longer than those for typical Yb^{3+}-doped fluoride laser hosts with τ ranging typically from 1.5 to 3 ms. This indicates the potential of highly-doped Yb^{3+}:Cs_2NaYF_6 crystals (up to 100 at%) for generation of high pulse energies in the Q-switched operation mode.

Gain cross-sections spectra for a 10 at% Yb^{3+}:Cs_2NaYF_6 crystal are shown in Fig. 5(b). For low inversion ratios ($\beta < 0.1$), the gain spectrum is flat and it spans from 1000 to 1080 nm, so the multi-peak spectral behavior is expected. For high inversion, two intense local peaks centered at $\sim$992 nm and 1009 nm are observed. This indicates the possibility of dual-wavelength laser operation for this crystal.

The lifetimes of the Yb^{3+} $^2F_{5/2}$ excited-state and the $^4I_{13/2}$ and $^4I_{11/2}$ excited-states for Er^{3+} ions are presented in Table 3. In this context, it is worth mentioning that even for a stoichiometric Cs_2NaErF_6 crystal, the value of $\tau(^4I_{11/2})$ is as long as 0.7 ms at room-temperature [5], which indicates that it can be promising medium for $\sim$3 μm laser operation on the $^4I_{11/2} \rightarrow {}^4I_{13/2}$ transition [25].

UCL spectra of Er^{3+}:Cs_2NaYF_6 crystals under the excitation at 960 nm to the Er^{3+} $^4I_{11/2}$ state are shown in Fig. 7(a). For a 10 at% Er^{3+} doped crystal, the green emission band spanning from 510 to 580 nm and related to the transitions from the closely located and thermalized state $^2H_{11/2}$ and $^4S_{3/2}$ to the ground state $^4I_{15/2}$

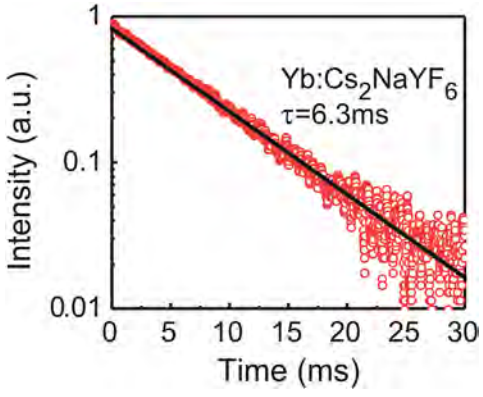

Fig. 6. Luminescence decay curve for a 10 at% Yb^{3+}:Cs_2NaYF_6 crystal: $\lambda_{exc} = 960$ nm; luminescence is detected at 1020 nm.

Table 3
Lifetimes of the excited-states of Er^{3+} and Yb^{3+} ions in Cs_2NaYF_6 crystals*.

Ion concentration	Yb^{3+} ion $\tau(^2F_{5/2})$, ms		Er^{3+} ion $\tau(^4I_{13/2})$, ms		Er^{3+} ion $\tau(^4I_{11/2})$, ms	
	This work/ RT	[6]/RT	This work/ RT	[5]/4 K	[5]/RT	[5]/4 K
1 at%	–	–	–	100	12	21
10 at%	6.3; 6.4_{rec}	–	$\sim 32_{rec}$	–	1.1	1.4
100 at%	5.7	5.63	–	–	0.7	1.1

* RT - room temperature, REC - estimated with the reciprocity method.

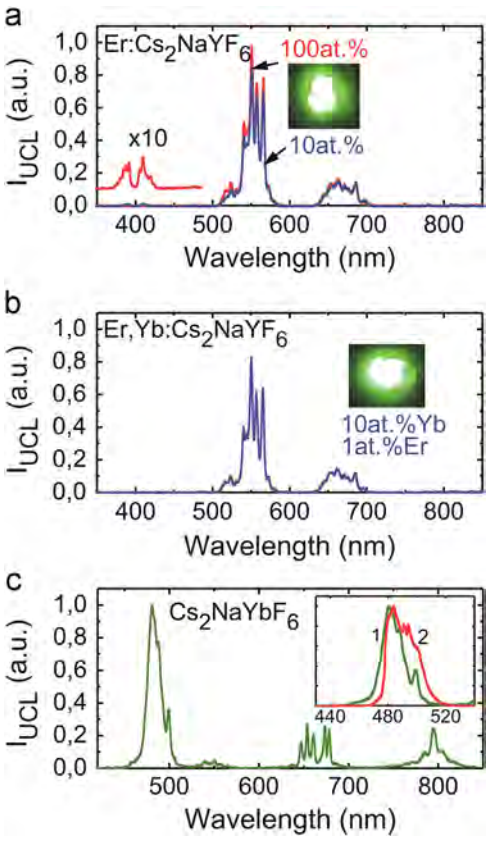

Fig. 7. Up-conversion luminescence (UCL) spectra for (a) 10 at% Er^{3+}:Cs_2NaYF_6 and Cs_2NaErF_6, (b) 1 at% Er^{3+}, 10 at% Yb^{3+}:Cs_2NaYF_6 and (c) Cs_2NaYbF_6 crystals; λ_{exc}=960 nm; *insets* show images of the excited samples (a), (b) and details of blue emission from the Cs_2NaYbF_6 crystal (c): 1-measured UCL spectrum, 2-calculated spectrum of cooperative emission, Eq. (6).

dominates in the spectrum. Four intense peaks at 540, 551, 557 and 566 nm are observed within this emission band. The red emission in the range 630–700 nm related to the transition $^4F_{9/2}\rightarrow$ $^4I_{15/2}$ is much weaker than the green one. The ratio for integrated intensities of these bands (R/G ratio) is 0.27 which is referred to the domination of the excited-state absorption (ESA) over the cross-relaxation (CR) mechanism in generation of UCL, however, further time-resolved studies of UCL are required to support this [26]. In the blue region there is a weak emission band which is due to the transition from the higher-lying excited state $^2H_{9/2}$ to the $^4I_{15/2}$ ground-state.

These features determine the yellow-green color of UCL from 10 at% Er^{3+}:Cs_2NaYF_6 with x=0.385 and y=0.603 in the 1931 CIE chromaticity coordinates as well as high color purity, $p>98\%$, caused by the dominant wavelength at 562 nm. Color purity p was calculated from the CIE 1931 chromaticity diagram with respect to the CIE-E illuminant (uniform white, x=0.333 and y=0.333). It is defined as $p=a/b$ where a is the distance from the white point to the sample color point and b is the distance from the white point to the point on the spectral locus corresponding to the dominant wavelength. The color purity is a quantitative measure of the saturation of a particular color. For a stoichiometric Cs_2NaErF_6 crystal and a 1 at% Er^{3+}, 10 at% Yb^{3+}:Cs_2NaYF_6 crystals, very similar UCL spectra are observed, see Fig. 7. Color characteristics for UCL from the studied crystals are summarized in Table 4.

In addition, UCL from a stoichiometric Cs_2NaYbF_6 crystal has been studied under the excitation at 960 nm to the Yb^{3+} $^2F_{5/2}$ state. The emission bands observed in Fig. 7(c) are due to ET from Yb^{3+} to impurity Tm^{3+} and Er^{3+} ions and UCL from Tm^{3+} dominates. Both Tm and Er are presented as trace impurities in ytterbium oxide, Yb_2O_3, reagent and thus their amount in stoichiometric crystal is enough to provide detectable UCL. The bands at 450–505, 640–680 and 750–820 nm are related to the transitions $^1G_4\rightarrow{}^3H_6$, $^1G_4\rightarrow{}^3F_4$ and $^3H_4\rightarrow{}^3H_6$ for Tm^{3+}, respectively, whereas weak green Er^{3+} emission from the $^2H_{11/2}$ and $^4S_{3/2}$ states to the $^4I_{15/2}$ ground state is detected at $\sim$550 nm. The red Er^{3+} emission from the $^4F_{9/2}$ state at $\sim$650 nm can overlap with the red Tm^{3+} one, so it is not discovered. Accordingly, UCL from the Cs_2NaYbF_6 crystal is blue–violet.

In the previous study of a Cs_2NaYbF_6 crystal [6], the strong emission bad at $\sim$480 nm is at least partially attributed to cooperative emission from Yb^{3+}–Yb^{3+} ion pairs [27]. This effect is known for materials with the strong clustering of Yb^{3+} ions [28]. In this case, a pair of closely located ions can form a virtual excited state with the energy $2E(^2F_{5/2})$ $\sim$20,000 cm^{-1}. The emission from this state can be observed in the region 480–500 nm [29]. The emission spectrum can be calculated as the convolution of the near-IR emission spectrum of Yb^{3+} ions related to the $^2F_{5/2}\rightarrow{}^2F_{7/2}$ transition [27]:

$$F_{coop}(E)=\int F_{IR}(E')F_{IR}(E-E')dE'. \quad (6)$$

The result of this calculation is presented in the inset of Fig. 7(c). The cooperative emission should occur in the spectral range 475–510 nm with a maximum at $\sim$484 nm that is very close to the maximum of the $^1G_4\rightarrow{}^3H_6$ Tm^{3+} emission in the Cs_2NaYF_6 crystal [3]. Thus, it is difficult to distinguish these effects spectrally. In [6] it has been found that the decay time of blue emission from a Cs_2NaYbF_6 crystal is 2.73 ms, which is almost exactly half of $\tau(^2F_{5/2})$ measured at $\sim$1 μm for Yb^{3+} ions. Such a correlation is expected for cooperative emission, $\tau_{coop}=\tau_{IR}/2$. Thus, blue UCL may be attributed to both Tm^{3+} impurity centers and cooperative emission. It should be also noticed that such intense UV up-conversion emissions can contribute to enhance the spectral response of photocatalytic semiconductor electrodes used in water-splitting processes for sustainable production of hydrogen, since they can help in bridging large bands gaps of efficient photocatalysts, like α-Fe_2O_3 (hematite), located at around 560 nm and eventually increase the efficiency of photoelectrochemical devices.

Table 4
CIE 1931 color coordinates x, y, dominant wavelength λ_d and color purity p for luminescence from Er^{3+} – doped elpasolite crystals.

Crystal	x	y	λ_d, nm	p	Color
Exc. 960 nm					
10 at% Er^{3+}:Cs_2NaYF_6	0.385	0.603	562	98%	Yellow–green
Cs_2NaErF_6	0.343	0.656	556	99%	Yellowish–green
1 at% Er^{3+}, 10 at% Yb^{3+}: Cs_2NaYF_6	0.340	0.660	555	99%	Yellowish–green
Exc. 355 nm					
10 at% Er^{3+}:Cs_2NaYF_6	0.333	0.650	555	99%	Yellowish–green
Cs_2NaErF_6	0.325	0.586	553	75%	Yellowish–green

In Fig. 8(a), log–log plots for the UCL intensity (I_{UCL}) versus the excitation power P are shown for a Cs_2NaErF_6 crystal. For the up-conversion process, I_{UCL} is proportional to the nth power of P, i.e. $I_{UCL} \sim P^n$ [30] where n is the number of pump photons absorbed per up-converted photon emitted. A plot of log I_{UCL} versus log P yields a straight line with slope n. For green emissions that occur from the $^2H_{11/2}$ and $^4S_{3/2}$ states, for the slope of this dependence $n=2.1$ (524 nm) and 1.9 (557 nm), which means that two pump photons are required to populate the above mentioned states. There is the same situation for red emission from the $^4F_{9/2}$ state at 660 nm where $n=2.1$. Normally, excitation of Er^{3+} ions to the higher lying excited states is achieved in two steps, for example ground-state absorption (GSA) $^4I_{15/2} \rightarrow {}^4I_{11/2}$ followed by excited-state absorption (ESA) from the $^4I_{11/2}$ or the $^4I_{13/2}$ states. For Cs_2NaErF_6, cross-relaxation (CR) between the adjacent Er^{3+} ions, which can participate as an additional mechanism for the population of the $^4F_{9/2}$ state, seems to be very weak. Indeed, the R/G ratio for UCL is not enhanced when the Er^{3+} concentration in Cs_2NaYF_6 increases from 10 to 100 at%, Fig. 7(a). This well correlates with the large distance between the isolated Y^{3+} sites in the Er^{3+}:Cs_2NaYF_6 crystal, so the probability of CR is not varied with the increase of the Er^{3+} concentration in the elpasolite hosts. No significant dependence of R/G ratio on the excitation power was detected.

Similar slopes ($n \sim 2$) for the log–og plots of the UCL intensity vs. the excitation power are observed also for a 1 at% Er^{3+}, 10 at% Yb^{3+}:Cs_2NaYF_6 crystal, Fig. 8(b). In this case, the first step of the UCL mechanism is the excitation of Er^{3+} ions through the GSA $^2F_{7/2} \rightarrow {}^2F_{5/2}$ of Yb^{3+} ions and the energy-transfer from Yb^{3+} to Er^{3+}, $^2F_{5/2}(Yb^{3+}) \rightarrow {}^4I_{11/2}(Er^{3+})$. On the other hand, in any case, 2 pump infrared photons are required for the generation of one visible photon. More detailed discussion about the mechanisms of UCL in hosts containing Er^{3+} and Yb^{3+} can be found elsewhere [31].

In Fig. 8(a), the I_{UCL} vs P plot for the blue UCL from a Cs_2NaYbF_6 crystal is also presented and the slope of this straight line is 2.4. This value is intermediate between the theoretical value of 2 for pure cooperative emission and 3 for pure Tm^{3+} $^1G_4 \rightarrow {}^3H_6$ emission. This supports our idea that the blue emission from the Cs_2NaYbF_6 crystal is due to the both processes.

Under excitation into the $^2G_{9/2}$ or the $^2H_{11/2}$ states of Er^{3+} in Cs_2NaYF_6 at 355 nm or 520 nm, respectively, all the crystals singly doped with Er^{3+} ions demonstrate emission spectra similar to those obtained under near-IR excitation, Figs. 9(a), 3(a) and 7(a). The corresponding color coordinates can be found in Table 4. However, for a 1 at% Er^{3+}, 10 at% Yb^{3+}:Cs_2NaYF_6 crystal the spectra are different from those of Er^{3+} doped Cs_2NaYF_6 crystals. In particular, a broad emission band spanning from 940 to 1050 nm is detected. This band is clearly different from the luminescent band related to the $^4I_{11/2} \rightarrow {}^4I_{15/2}$ transition of Er^{3+} ions and has the spectral features of emission on the Yb^{3+} $^2F_{5/2} \rightarrow {}^2F_{7/2}$ transition. Excitation of Yb^{3+} ions is due to the so-called down-conversion ("quantum cutting") process for the Er^{3+}–Yb^{3+} ion pairs [32,33].

It should be also noted that enhancement of the efficiency of the up- and down- conversion processes in cubic elpasolites is possible with the ytterbium compositions $Cs_2NaEr_xYb_{1-x}F_6$ containing relatively high Er^{3+} concentrations.

4. Conclusions

To conclude, we have studied absorption and luminescence of Er^{3+} and Yb^{3+} ions in cubic elpasolite Cs_2NaYF_6 crystals as well as in crystals of Cs_2NaErF_6 and Cs_2NaYbF_6 synthesized under hydrothermal conditions. Stimulated-emission and gain cross-sections have been determined for the Yb^{3+} $^2F_{5/2} \rightarrow {}^2F_{7/2}$ and the Er^{3+} $^4I_{13/2} \rightarrow {}^4I_{15/2}$ transitions in 10 at% Yb^{3+}:Cs_2NaYF_6 and 10 at% Er^{3+}:Cs_2NaYF_6 at room temperature. The maximum σ_{SE} values are 1.8×10^{-21} cm^2 at 993 nm (Yb^{3+}) and 3.8×10^{-21} cm^2 at 1535 nm (Er^{3+}). The possibility of dual-wavelength laser operation and wide tuning range exceeding 100 nm for laser emission are

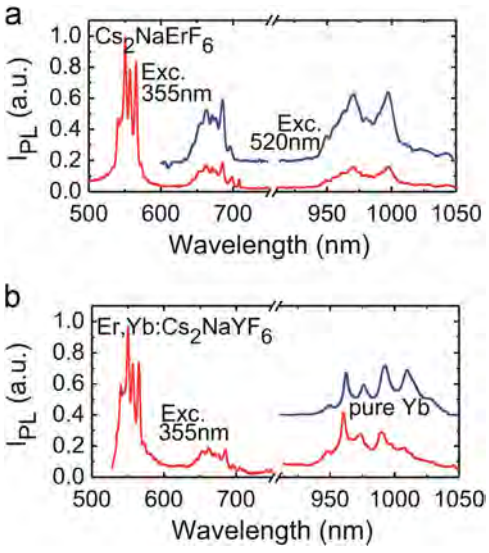

Fig. 9. Luminescence of Cs_2NaErF_6 (a) and 1 at% Er^{3+}, 10 at% Yb^{3+}:Cs_2NaYF_6 (b) crystals after excitation into the $^2G_{9/2}$ state at 355 nm and into the $^2H_{11/2}$ state at 520 nm; the spectrum of Yb^{3+} emission from the Cs_2NaYbF_6 crystal is added in (b) for comparison.

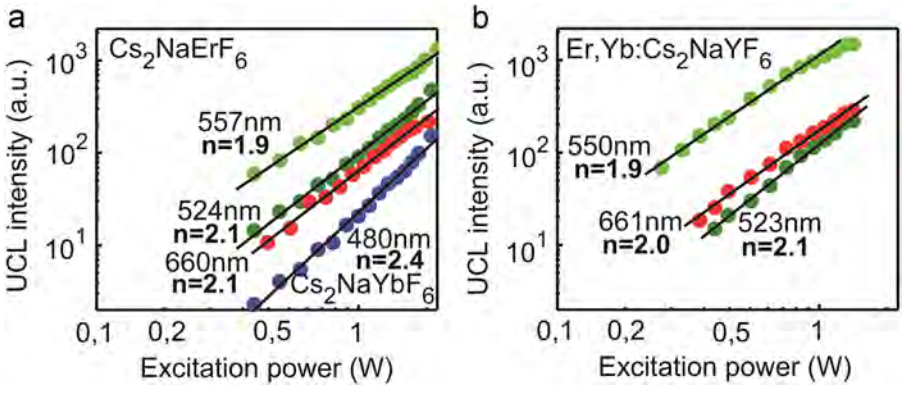

Fig. 8. Dependences of the UCL intensity on the excitation power in a log–log scale for (a) Cs_2NaErF_6, Cs_2NaYbF_6 and (b) 1 at% Er^{3+}, 10 at% Yb^{3+}:Cs_2NaYF_6 (b) crystals; $\lambda_{exc}=960$ nm; n is the number of pump photons absorbed per up-converted photon emitted.

expected for Yb^{3+}:Cs_2NaYF_6 crystals. Due to their structure peculiarities, elpasolite crystals provide exceptionally long radiative lifetimes of the excited-states for both $Yb^{3+}$and Er^{3+}ions, τ ($^2F_{5/2}$)=6.3 ms and τ($^4I_{13/2}$) ~32 ms, respectively, together with relatively weak UCL, which makes them attractive for high pulse energy Q-switched lasers. Under excitation at 960 nm, Cs_2NaErF_6 crystals provide yellowish–green UCL with CIE coordinates x=0.353, y=0.656. Down-conversion is detected for Er^{3+},Yb^{3+}:Cs_2NaYF_6 crystals.

Acknowledgments

This research was partially supported by the Russian Foundation for Basic Research (Research Project no. 15-03-02507a); Fundación CajaCanarias (AYE06) within the Project MAGEC (Materials for Advanced Generation of Energy at Canary Islands) and the Spanish Ministry of Economy and Competitiveness (Project ENE2013-47826-C4-4-R).

References

[1] G. Meyer, Prog. Sol. St. Chem. 14 (1982) 141.
[2] L.R. Moras, J. Inorg. Nucl. Chem. 36 (1974) 3876.
[3] V.N. Makhov, N.M. Khaidukov, D. Lo, J.C. Krupa, M. Kirm, E. Negodin, Opt. Mater. 27 (2005) 1131.
[4] X. Zhou, P.A. Tanner, M.D. Faucher, J. Phys. Chem. C 111 (2007) 683.
[5] H. Vrielinck, I. Izeddin, V.Y. Ivanov, T. Gregorkiewicz, F. Callens, D.S. Lee, A.J. Steckl, N.M. Khaidukov, Mater. Res. Soc. Symp. 866 (2005) V381.
[6] D.S. Pytalev, A. Jaffres, P. Aschehoug, P.A. Ryabochkina, A.V. Malov, N.M. Khaidukov, M.N. Popova, J. Lumin. 153 (2014) 125.
[7] M.L. Falina, K.I. Gerasimova, A.M. Leushin, N.M. Khaidukov, J. Lumin. 128 (2008) 1103.
[8] X. Zhou, M.F. Reid, M.D. Faucher, P.A. Tanner, J. Phys. Chem. B 110 (2006) 14939.
[9] B.Z. Malkin, D.S. Pytalev, M.N. Popova, E.I. Baibekov, M.L. Falin, K.I. Gerasimov, N.M. Khaidukov, Phys. Rev. B 86 (2012) 134110.
[10] P.A. Tanner, M.D. Faucher, Chem. Phys. Lett. 445 (2007) 183.
[11] P.A. Tanner, Y.L. Liu, N. Edelstein, K. Murdoch, N.M. Khaidukov, J. Phys. : Condens. Matter 9 (1997) 7817.
[12] J.R.G. Thorne, M. Jones, C.S. McCaw, K.M. Murdoch, R.G. Denning, N.M. Khaidukov, J. Phys. : Condens. Matter 11 (1999) 7851.
[13] A.J. Berry, I.D. Morrison, R.G. Denning, Mol. Phys. 93 (1998) 1.
[14] W. Ryba-Romanowski, Z. Mazurak, B. Jezowska-Trzebiatowska, J. Lumin. 27 (1982) 177.
[15] P.A. Tanner, C.S.K. Mak, W.-M. Kwok, D.L. Phillips, M.D. Faucher, Phys. Rev. B 66 (2002) 165203.
[16] Z. Mazurak, E. Lujowiak, B. Jezowska-Trzebiatowska, W. Ryba-Romanowski, J. Lumin. 29 (1984) 47.
[17] Z. Mazurak, E. Lujowiak, B. Jezowska-Trzebiatowska, J. Lumin. 33 (1985) 159.
[18] F. Auzel, Chem. Rev. 104 (2004) 139.
[19] G.N. Papatheodorou, J. Chem. Phys. 66 (1977) 2893.
[20] S.A. Payne, L.L. Chase, L.K. Smith, W.L. Kway, W.F. Krupke, IEEE J. Quant. Electron. 28 (1992) 2619.
[21] P.A. Loiko, E.A. Arbabzadah, M.J. Damzen, X. Mateos, E.B. Dunina, A.A. Kornienko, A.S. Yasukevich, N.A. Skoptsov, K.V. Yumashev, J. Lumin. 171 (2016) 226.
[22] A.S. Yasyukevich, V.G. Shcherbitskii, V.E. Kisel, A.V. Mandrik, N.V. Kuleshov, J. Appl. Spectr. 71 (2004) 202.
[23] P.A. Tanner, Mol. Phys. 63 (1988) 365.
[24] B.F. Aull, H.P. Jenssen, IEEE J. Quantum Electron. 18 (1982) 925.
[25] B.J. Dinerman, P.F. Moulton, Opt. Lett. 19 (1994) 1143.
[26] J. Mendez-Ramos, V. Lavin, I.R. Martin, U.R. Rodriguez-Mendoza, J.A. Gonzalez-Almeida, V.D. Rodriguez, A.D. Lozano-Gorrin, P. Nunez, J. Alloy. Compd. 323–324 (2001) 753.
[27] Ph Goldner, F. Pelle, D. Meichenin, F. Auzel, J. Lumin. 71 (1997) 137.
[28] F. Auzel, D. Meichenin, F. Pellé, P. Goldner, Opt. Mater. 4 (1994) 35.
[29] P.A. Loiko, G.E. Rachkovskaya, G.B. Zakharevich, A.A. Kornienko, E.B. Dunina, A.S. Yasukevich, K.V. Yumashev, J. Non-Cryst. Solids 392–393 (2014) 39.
[30] M. Pollnau, D.R. Gamelin, S.R. Luthi, H.U. Gudel, Phys. Rev. B 61 (2000) 3337.
[31] P.A. Loiko, N.M. Khaidukov, J. Méndez-Ramos, E.V. Vilejshikova, N.A. Skoptsov, K.V. Yumashev, J. Lumin. 170 (2015) 1.
[32] L. Aarts, B.M. van der Ende, A. Meijerink, J. Appl. Phys. 106 (2009) 023522.
[33] J.J. Eilers, D. Biner, J.T. van Wijngaarden, K. Krämer, H.-U. Güdel, A. Meijerink, Appl. Phys. Lett. 96 (2010) 151106.